ACS OMEGA

http://pubs.acs.org/journal/acsodf

Article

# Conjugation of Ctx(Ile$^{21}$)-Ha Antimicrobial Peptides to Chitosan Ultrathin Films by *N*-Acetylcysteine Improves Peptide Physicochemical Properties and Enhances Biological Activity

Cesar Augusto Roque-Borda, Bruna Fernandes Antunes, Anna Beatriz Toledo Borgues, Janaína Teixeira Costa de Pontes, Andréia Bagliotti Meneguin, Marlus Chorilli, Eliane Trovatti, Silvio Rainho Teixeira, Fernando Rogério Pavan, and Eduardo Festozo Vicente*

Cite This: *ACS Omega* 2022, 7, 28238−28247

Read Online

ACCESS | Metrics & More | Article Recommendations

**ABSTRACT:** The importance of obtaining new compounds with improved antimicrobial activity is a current trend and challenge. Some polymers such as chitosan have shown promising bactericidal properties when they are structurally modified, which is due to the binding versatility provided by their free amines. Likewise, antimicrobial peptides (AMPs) have received attention in recent years because of their bactericidal activity that is similar to or even better than that of conventional drugs, and they exhibit a low induction rate of antimicrobial resistance. Herein, the modified AMP Ctx(Ile$^{21}$)-Ha-Ahx-Cys was conjugated to chitosan using *N*-acetylcysteine as an intermediate by the carbodiimide method. Films were prepared using protonated chitosan in 1% acetic acid and Ctx(Ile$^{21}$)-Ha-Ahx-Cys AMP dissolved in *N*-acetylcysteine-chitosan; 1.6 mmol of ethylcarbodiimide hydrochloride, 1.2 mmol of *N*-hydroxysulfosucchimide, and 0.1 mol L $^{-1}$of *N*-morpholino)ethanesulfonic acid buffer at pH 6.5 by continuous stirring at 100 × g for 10 min at 37 °C. Physicochemical properties were evaluated by Fourier-transform infrared spectroscopy, differential scanning calorimetry/thermogravimetric analysis, and X-ray diffraction to determine the mechanical properties, solubility, morphology, and thickness. Furthermore, the antimicrobial activities of chitosan-based conjugated films were evaluated against*Staphylococcus aureus*,*Pseudomonas aeruginosa*,*Salmonella*Typhimurium, and *Escherichia coli*. The results showed that the conjugation of a potent AMP could further increase its antibacterial activity and maintain its stable physicochemical properties. Therefore, the developed peptide−chitosan conjugate could be applied as an additive in surgical procedures to prevent and combat bacterial infection.

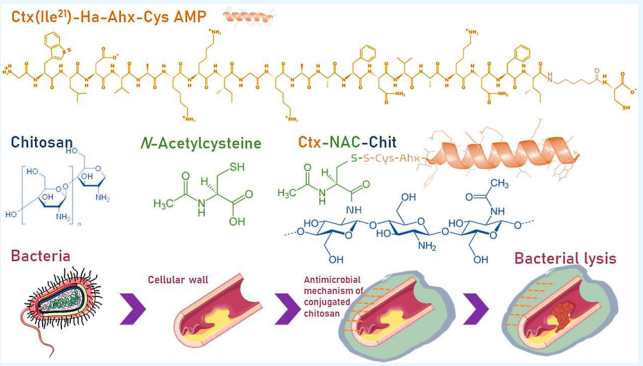


## 1. INTRODUCTION

The use of biopolymers with antimicrobial activity is increasingly studied due to their high biocompatibility, bioavailability, and versatility.[1] Chitosan, derived from partially or totally deacetylated chitin, is an easily accessible, biodegradable cationic polymer that has interesting antimicrobial characteristics.[2] The antimicrobial action mechanism of chitosan is still not fully understood. However, it has been revealed that, during its application, several cellular events may occur: modification of the cell membrane/cell wall, interaction with microbial DNA, chelation of nutrients, or formation of dense polymeric films on the cell surface, thus achieving cell lysis.[3] Chitosan is a polysaccharide made up of D-glucosamine linked to $\beta$-(1-4) and *N*-acetyl-D-glucosamine, which has free amine radicals in its structure and is essential for obtaining conjugated molecules or derivatives, such as carboxymethyl chitosan, *N*,*N*,*N*-trimethyl chitosan, and *N*-acetyl-L-cysteine-chitosan (NAC-Chit), among others.[4] NAC-Chit is a derivative that has improved mucoadhesive and cohesive properties relative to the original chitosan. The union of chitosan and *N*-acetyl-L-cysteine occurs through the primary amino group of chitosan and a carboxylic acid group of the sulfhydryl compound that is activated by a carbodiimide method.[5]

On the other hand, antimicrobial peptides (AMPs) are biomacromolecules that have received special attention because many of them are potential destabilizers of the

Received: April 25, 2022
Accepted: July 20, 2022
Published: August 5, 2022

bacterial wall, interacting mainly with the lipopolysaccharides that are part of their composition.[6] AMPs have several mechanisms of action that can cause bacterial lysis; some may act directly with the bacterial membrane as well as insert and accumulate within the cytoplasm to alter some of the metabolic pathways of DNA (replication, transcription, translation, etc.).[7] The interaction of the bacterial membrane can be explained by the barrel-stave model, where the peptides are grouped in three different ways: in a bilayer that separates the hydrophobic peptides aligned with the lipid center and the hydrophilic end that creates an opening inside the membrane; in the toroidal model, whereby peptides accumulate and cause the lipid layer to fold to form pores; or in the carpet model, whereby peptides create an opening in the outer membrane.[8] The AMPs showed efficacy even against multidrug-resistant (MDR) bacteria and clinical isolates.[9] In particular, a peptide isolated from frog skin, known as Ctx(Ile$^{21}$)-Ha, has shown excellent biological activity against bacteria of public health concern such as *Escherichia coli*, *Pseudomonas aeruginosa*, *Staphylococcus aureus*, and *Candida albicans*.[10] However, its direct systemic application could be difficult because this molecule has shown higher hemolytic activity. It was previously demonstrated that Ctx(Ile$^{21}$)-Ha AMP encapsulated in alginate microparticles and coated with cellulose derivatives managed to reduce its hemolytic activity and that its structure also remained stable during its application in the gastrointestinal tract.[11,12] Therefore, several strategies may be used to enhance the activity of AMPs and improve their stability in biological systems, among which is their bioconjugation.[13,14]

In this way, to improve the antimicrobial effect using low peptide concentration, this study proposed to develop an ultrathin film based on *N*-Acetyl-L-cysteine (NAC)-chitosan conjugated with a strategically modified sequence of Ctx-(Ile$^{21}$)-Ha AMP and subsequently evaluate its characterization, physicochemical properties, and antimicrobial activities.

## 2. MATERIALS AND METHODS

**2.1. Chemical Reagents.** Chitosan and Tris-HCl were obtained from Êxodo Científica (São Paulo, Brazil); amino acids, resin (Fmoc-Rink amide resin), 4-methylpiperidine, hydroxybenzotriazole (HOBt), *N*,*N*′-diisopropylcarbodiimide (DIC), trifluoroacetic acid (TFA), triisopropylsilane (TIS), ethanedithiol (EDT), NAC, *N*′-ethylcarbodiimide hydrochloride (EDC), *N*-hydroxysulfosucchimide (NHS), (*N*-morpholino)ethanesulfonic acid (MES), dimethyl sulfoxide (DMSO), acetonitrile, and triethyl citrate were obtained in high-performance liquid chromatography grade from Sigma-Aldrich (St Louis, USA); dimethylformamide (DMF) was purchased from Neon Comercial (São Paulo, Brazil); dichloromethane (DCM) was purchased from Anidrol Laboratory (São Paulo, Brazil).

**2.2. Synthesis of the Antimicrobial Peptide Ctx(Ile$^{21}$)-Ha.** AMP (free carboxylate C-terminus) was synthesized and assembled by standard Fmoc/*t*Bu solid-phase peptide synthesis methodologies, with manual assistance. At the C-terminal original sequence of the Ctx(Ile$^{21}$)-Ha AMP (GWLDVAK-KIGKAAFAVAKNFI, hereafter Ctx), the spacer Fmoc-6-Ahx-OH (6-(Fmoc-amino)hexanoic or caproic acid) and a cysteine residue were inserted to enable the attachment of the resulting Ctx(Ile$^{21}$)-Ha-Ahx-Cys molecule to NAC-Chit. Briefly, the Fmoc-Cys(Trt)-Wang resin was preconditioned for 15 min in DMF/DCM (3 times). The initial Fmoc-deprotection step was carried out using a solution of 20% 4-methylpiperidine in DMF. The C-terminal cysteine residue was then already coupled to the deprotected Wang resin. Then, the spacer Fmoc-6-Ahx-OH was used in the next coupling with 0.6 M equivalents (eq) in the next Fmoc-protected amino acid couplings and with 0.6 eq HOBt-DIC in 1:1 v/v DMF/DCM. The coupling steps were carried out for 2 h at room temperature (RT) by stirring. Therefore, the remaining amino acids were sequentially coupled in the C → N direction by means of similar deprotection and coupling cycles. The Kaiser test was performed to monitor the coupling completeness. After the end of the sequence assembly, the peptide was released from the resin with the concomitant removal of side-chain protecting groups by hydrolysis using a cocktail containing TFA, TIS, EDT, and water (94:1:2.5:2.5 v/v/v/v) as scavengers for 2 h at RT. Then, samples were lyophilized (Liotop, model K108, Brazil) until a powder was formed.[11]

**2.3. Peptide Purification and Characterization.** The degree of peptide purity was checked by analytical high-performance liquid chromatography (HPLC). For Ctx(Ile$^{21}$)-Ha-Ahx-Cys purification, samples were injected in an analytical HPLC system (Shimadzu Prominence, with a membrane degasser DGU-20A5R, a UV detector SPD-20A, a column oven CTO-20A, an automatic sampler SIL-10AF, a fraction collector FRC-10A, and an LC-20AT dual-pump) with a reverse-phase Shimadzu C18 column at a flow rate of 1 mL min$^{-1}$ using solvents 0.045% TFA in aqueous solution (eluent A) and 0.036% TFA in acetonitrile (eluent B) for 30 min. Subsequently, pure peptide fractions were collected and pooled, freeze-dried, and stored at −20 °C until use. To confirm that the molecule was obtained, characterization by LC−MS analyses was performed on a Shimadzu chromatograph/Bruker spectrometer (Prominence/Amazon SL) with the same parameters as those used for the HPLC purification system at a flow rate of 0.5 mL min$^{-1}$ using a gradient method of 5 to 95% of eluent B for 30 min. All samples were analyzed in a dual-wavelength mode at 220/280 nm, and the Ctx(Ile$^{21}$)-Ha-Ahx-Cys peptide molecule was only used if 95% or a higher degree of purity was reached. The theoretical molecular weight of the Ctx(Ile$^{21}$)-Ha-Ahx-Cys peptide is 2504 g mol$^{-1}$.

**2.4. Chitosan Preparation and Purification.** The protonated chitosan (Chit) was purified using the reprecipitation method.[15] Briefly, 0.5% of chitosan dissolved in Milli-Q water was kept at 4 °C for 24 h with constant and gentle magnetic stirring. After this procedure, 1% of acetic acid was added and mixed overnight at RT, resulting in a gel solution, which was then filtered using 20 $\mu$m pore-size filters to eliminate undissolved particles. Reprecipitation was carried out with 1 M NaOH solution at RT under constant stirring. Finally, the obtained material was washed with Milli-Q water and centrifuged. This procedure was repeated 5 times to reach a neutral pH until the material was lyophilized.

**2.5. Synthesis of Modified Chitosan.** Chitosan was modified by using *N*-acetyl-L-cysteine in chitosan (NAC-Chit) according to Costa et al.[15] Briefly, 0.5 g of purified chitosan was added to 1% acetic acid in a volume of 16 mL and homogenized until complete dissolution. Then, a solution was prepared with 1.6 mM of EDC, 1.2 mM of NHS, and 0.1 M of MES buffer at pH 6.5 by continuous stirring at 100 × g at 37 °C for 10 min. Finally, 160 mg of NAC was added to the previous solution for 2 h under the same conditions.

**2.6. Synthesis of the Ctx-NAC-Chit Conjugate.** The formation of the disulfide bridge between the thiol group from


https://doi.org/10.1021/acsomega.2c02570
ACS Omega 2022, 7, 28238−28247

the side chain of the C-terminal cysteine residue of the peptide and the sulfhydryl groups (SH) in the functionalized chitosan-NAC was carried out using 10 mg of the Ctx(Ile$^{21}$)-Ha-Ahx-Cys peptide at pH 8 in Tris-HCl buffer and 20% DMSO (w/v) at 37 °C and 120 rpm for 18 h. The conjugated samples were reprecipitated using a 1 M NaOH solution at RT with constant stirring, washed with Milli-Q water, and centrifuged 3 times. Samples from all conjugation stages were always lyophilized, and for characterization studies, they were resolubilized with 1% acetic acid for 24 h at RT.

**2.7. Fourier-Transform Infrared Spectroscopy Analysis.** The Fourier-transform infrared spectroscopy (FT-IR) spectra of microencapsulates were recorded using a spectrometer (PerkinElmer spectrometer, Frontier, USA). The samples were milled and mixed with dried KBr. The transmittance spectra of the microencapsulated powders were registered with a resolution of 4 cm$^{-1}$. Attenuated total reflectance spectra were obtained in a Bruker Vertex 70 FT-IR spectrometer. All the experimental data were analyzed in the range of 1800 to 400 cm$^{-1}$ wavelength numbers using OriginPro 2019b software.

**2.8. Film Solubility in Water.** The solubility of the chitosan ultrathin films in water was performed according to García et al.[16] Briefly, the conjugated films were cut into 3 cm × 2 cm fractions and dried for 7 days at 0% relative humidity. Subsequently, each film was placed in a beaker with 80 mL of water and homogenized using a magnetic stirrer at 110 rpm for 1 h at RT. Then, the remaining film was quickly dried in an oven at 60 °C until a constant weight was obtained. Finally, calculations were performed according to eq 1.

$$\%\ \text{solubility} = \frac{\text{Initial dry weight} - \text{Final dry weight}}{\text{Initial dry weight}} \times 100 \quad (1)$$

**3.9. Thermal Analysis.** The thermogravimetric analysis (TGA), associated with the derivative thermogravimetric analysis and differential scanning calorimetry (DSC), was also performed with the microparticles, pure peptide, and negative control. Approximately 10−12 mg of each type of sample was wrapped in an alumina crucible and kept under a synthetic air atmosphere with a flow rate of 100 mL min$^{-1}$ in the temperature range of 30 at 800/1000 °C at a heating rate of 5 °C min$^{-1}$. The results were obtained and processed with DSC-TGA equipment (SDT Q600 V20.9 Build 20, TA Instruments) with Universal Analysis 2000 software.

**3.10. X-ray Diffraction.** The crystallinity of the chitosan ultrathin films was studied by setting the parameters at 40 kV and 30 mA, Cu K$\alpha$1 ($\lambda$ = 1.5406 Å), and CuK$\alpha$2 ($\lambda$ = 1.5444 Å) radiation in an X-ray diffractometer (XRD-6000, Shimadzu). Divergence and receiving slots of 1° in the continuous scan mode, a scanning speed of 2°/min$^{-1}$, and an angular range of 2$\theta$ from 5° to 60° were used. The films were placed in an aluminum or glass sample holder depending on the amount of samples available. The diffraction spectra (or diffraction peaks) were identified using the powder diffraction files from the Joint Committee on Powder Diffraction Standards (JCPDS-ICDD) database.[11,17] The crystallinity index was estimated by following eq 2 proposed by Struszczyk.[18]

$$\text{CrI} = \frac{I_{110} - I_{am}}{I_{110}} \times 100 \quad (2)$$

where $I_{110}$ is the intensity around 17.54° (2$\theta$) as a crystalline domain and $I_{am}$ is the intensity around 12.96° (2$\theta$) as an amorphous domain.

**3.11. Morphology.** To analyze the conjugate morphology, a scanning electron microscope (JEOL Ltd., Japan) was employed. Chitosan ultrathin films were coated with charcoal after bonding with the ends of the tape. The surface of the samples was analyzed with a 2.0 kV energy emission current, a current probe of 9, and a 6.5 mm working distance in a secondary electron (SE) imaging mode at 10,000× magnification (1 pixel = 0.935 nm).

**3.12. Mechanical Properties.** The mechanical properties of the clamped and free films were evaluated using a TA-XT2 texture analyzer (Stable Micro Systems) with a spherical tip puncture probe (25 mm, constant speed of 1 mm s$^{-1}$) and a metal fixative with a circular hole ($D$ = 50 mm). The puncture strength (Ps), the elongation at break (Eb), and the puncture energy (Ep) were determined by obtaining the firing force (0.005 kg), and the force versus displacement curves were recorded until the film broke.[19] Equations 3−5 were used for these analyses, as described below

$$\text{Ps} = \frac{F}{A} \quad (3)$$

$$A = 2rh \quad (4)$$

$$\text{Eb}\% = \frac{\sqrt{r^2 - d^2} - r}{r} \times 100 \quad (5)$$

where $F$ (MPa) is the force required to break the film, $A$ (mm) is the area of the film section, $r$ (mm) is the hole radius, $h$ is the thickness of the film, and $d$ (mm) is the displacement.

**3.13. Antibacterial Activity.** The antimicrobial activity was evaluated using bacteria supplied by the Tuberculosis Laboratory of the Department of Biological Sciences of the FCF/UNESP. The pathogenic bacteria tested were *S. aureus* subsp. aureus Rosenbach (ATCC 25923), *P. aeruginosa* (Schroeter) Migula (ATCC 27853), *Salmonella enterica* subsp. enterica serovar Typhimurium (ATCC 14028), and *E. coli* (Migula) Castellani and Chalmers (ATCC 25922). All bacteria were cryopreserved in LB broth containing 50% glycerol and stored at −80 °C.

The minimal inhibitory concentration (MIC) of the Ctx(Ile$^{21}$)-Ha peptide and Ctx(Ile$^{21}$)-Ha-NAC-Chit-conjugated polymer-peptide against the strains was determined using the microdilution method, according to the requirements of the M100 manual.[20] The bacteria were thawed and reactivated in LB broth at 37 °C for 24 h. Subsequently, a suspension was obtained in the 0.5 McFarland scale using a DEN-1 densitometer (AKRALAB, Spain) for each strain. The wells were mounted in serial dilutions for the Ctx(Ile$^{21}$)-Ha-Ahx-Cys peptide at an initial concentration of 250 $\mu$g mL$^{-1}$ and a final dilution of 0.97 $\mu$g mL$^{-1}$.

For biological repetitions, the bacteria were recultivated in LB medium, and the same steps were followed. LB broth was prepared using 10 g L$^{-1}$ of tryptone, 5 g L$^{-1}$ of yeast extract, and 10 g L$^{-1}$ of NaCl, and LB medium was used at the same concentration with 15 g L$^{-1}$ of agar.

**3.14. Hemolytic Activity.** Hemolytic activity was used to determine the number of erythrocytes lysed after exposure to the conjugates according to Serrano et al.[21] Briefly, 1% triton was used as a positive control and PBS 1× as a negative control. The erythrocytes were washed with PBS 1× and


https://doi.org/10.1021/acsomega.2c02570
ACS Omega 2022, 7, 28238−28247

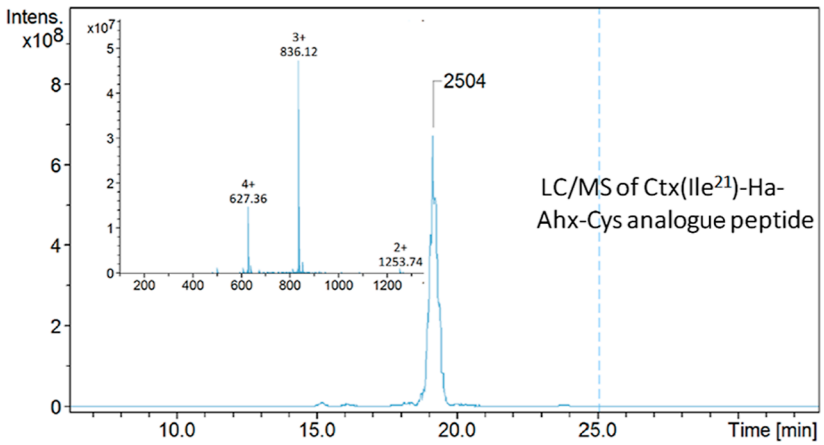


**Figure 1.** Chromatogram profile and *inset* peptide mass spectrometry spectra of the synthesized Ctx(Ile$^{21}$)-Ha-Ahx-Cys. Retention time of 19 min, molecular weight of 2504 g mol$^{-1}$, and purity greater than 95%.

centrifuged at 3000*g* for 3 min in triplicate. The samples were placed in a 96-well microplate at a concentration of 0.5 mg/mL (15 times the MICs) with the erythrocytes ($2 \times 10^6$ cells/mL) in a 1:1 ratio and incubated for 1 h. The results were analyzed on a microplate reader at an absorbance of 540 nm and calculated using eq 6.

$$\text{Hemolysis (\%)} = \frac{(A_s - A_b)}{(A_t - A_b)} \times 100 \quad (6)$$

where $A_s$ is the absorbance of the samples, $A_b$ is the mean of the absorbance in the buffer, and $A_t$ corresponds to the total lysis of the cells.

## 4. RESULTS AND DISCUSSION

**4.1. Synthesis, Purification, and Characterization of Ctx(Ile$^{21}$)-Ha-Ahx-Cys.** The modified Ctx(Ile$^{21}$)-Ha-Ahx-Cys AMP was correctly synthesized, purified, and characterized. The peak appears at the retention time of 19 min, confirming the mass/charge ratios of 627.36 ($Z$ = +4), 836.12 ($Z$ = +3), and 1253.74 ($Z$ = +2) in the spectrum, as shown in Figure 1. Subsequently, a peptide with a purity greater than 95% was obtained. The characterization of the Ctx(Ile$^{21}$)-Ha AMP original molecule was also previously reported, and it correlates very well with the literature.[10,11]

**4.2. FT-IR Spectroscopy Analysis.** For this study, chitosan (Chit) was used as a control. Modified chitosan (NAC-Chit) and chitosan conjugated with the peptide (Ctx-NAC-Chit) are shown in Figure 2.[22] Protonated chitosan, as well as many other carbohydrates, exhibited the band at 1078 cm$^{-1}$, suggesting symmetric carbonyl stretching of the glucose region. Likewise, 1,650.99 cm$^{-1}$ and 1,404.11 cm$^{-1}$ conferred an intensity ratio of amide I; in addition, a 1049.22 cm$^{-1}$ peak was formed, differentiating chitosan from NAC-Chit.[23] Together, the peptide grafted onto chitosan showed several bands that confirm the successful binding, such as the disulfide bridge formed between the cysteine thiol groups of the antimicrobial peptide and NAC-Chit at 526.54 cm$^{-1}$.[24]

The bands at 1596 and 1406 cm$^{-1}$ indicate the slight symmetric and antisymmetric movement of the free carboxylates, incorporating $\alpha$-helical. Furthermore, it is possible to visualize the vibrations of amide I distributions in 1652.91 cm$^{-1}$ ($\alpha$-helix); 1643.27 cm$^{-1}$ (enzymatic stability decreases when there is peptide digestion); 1633.63 cm$^{-1}$ ($\beta$-sheet); 1596.98 cm$^{-1}$ (antisymmetric stretching); and 1622.06 cm$^{-1}$ (solver-exposed $\beta$-sheet) from amide II at 1473.54 cm$^{-1}$ (asymmetric scissors in peptides and proteins);[23,25,26] from amide III at 1406.04 cm$^{-1}$ (symmetrical stretching of carboxylates that decreases when the molecule is more stable against proteolysis); 1396.39 cm$^{-1}$ (symmetrical stretching of COO- of proteins); 1377.11 cm$^{-1}$ (in chitosan, this signal is the key to the formation of new materials); and 1230.52 cm$^{-1}$ (secondary structure together with amide II).[25−27]

According to Costa et al.,[15] the relationship between bands 1654 cm$^{-1}$ (amide I) and 1085.87 cm$^{-1}$ (glucopyranose, C−O−C) indicates the modification in the structure since the bands increase their intensity when chitosan is modified with NAC. This effect is mainly due to the generation of amide groups (peptide bonds) from NAC carboxyl groups with the chitosan amine groups. The results of the relationship between 1654 and 1083 cm$^{-1}$ (Figure 2C) showed that Ctx-NAC-Chit is 2.15 times less than NAC-Chit, which confirms the covalent immobilization of the Ctx(Ile$^{21}$)-Ha peptide as a conjugate of chitosan and NAC.[15]

**4.3. Water Solubility Analysis.** The conjugated films showed low solubility in comparison with the original chitosan films (Table 1). However, significant differences were recorded between the reference chitosan and the conjugates. These differences may be due to NAC's having greater solubility in water, a property probably conferred by chitosan after being conjugated.[28] On the other hand, the peptide is amphipathic, which may hinder complete solubilization in water. In addition, its solubility did not increase significantly due to the small amount of peptide used for its insertion into the NAC-Chit.

**4.4. Thermal Studies.** Thermograms help us to distinguish and monitor the different thermal events as well as the thermal stability of each polymer modification. Figure 3 shows two important events of thermal degradation. The first one involved the complete elimination of the water that the chitosan film hygroscopically absorbs, and it occurred up to 150 °C through mass loss since critical events took place through the derivative of the TGA (dTGA). The results of the first dTGA event of NAC-Chit showed a mass loss of 18.95%, as opposed to Ctx-NAC-Chit, which exhibited a loss of 12.28%. Therefore, it is possible to deduce that its thermal properties were modified during its conjugation, offering greater resistance to degradation because the dTGA event translocated to the right ($T_{peak}$ 250 to 270 °C). The second event, which occurred at 150−~400 °C, could be related to


https://doi.org/10.1021/acsomega.2c02570
ACS Omega 2022, 7, 28238−28247

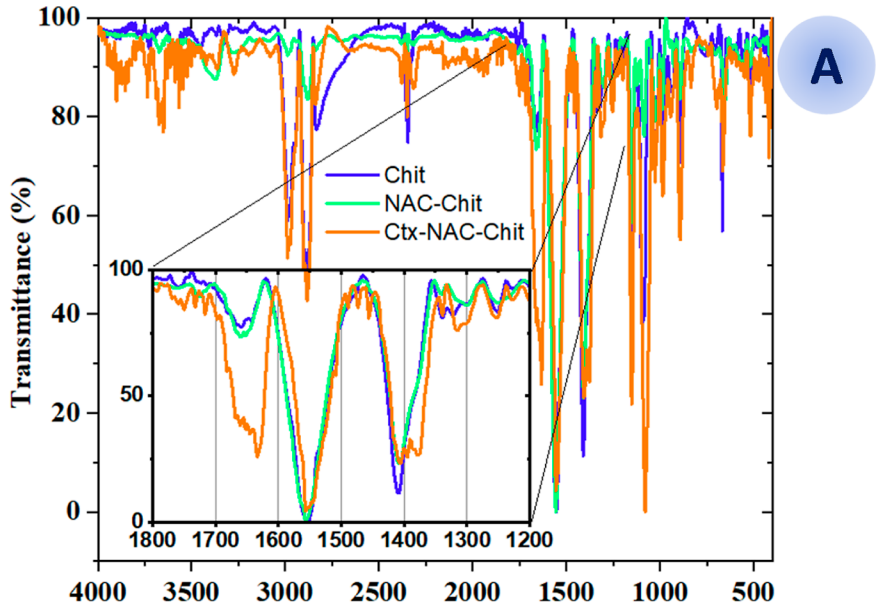


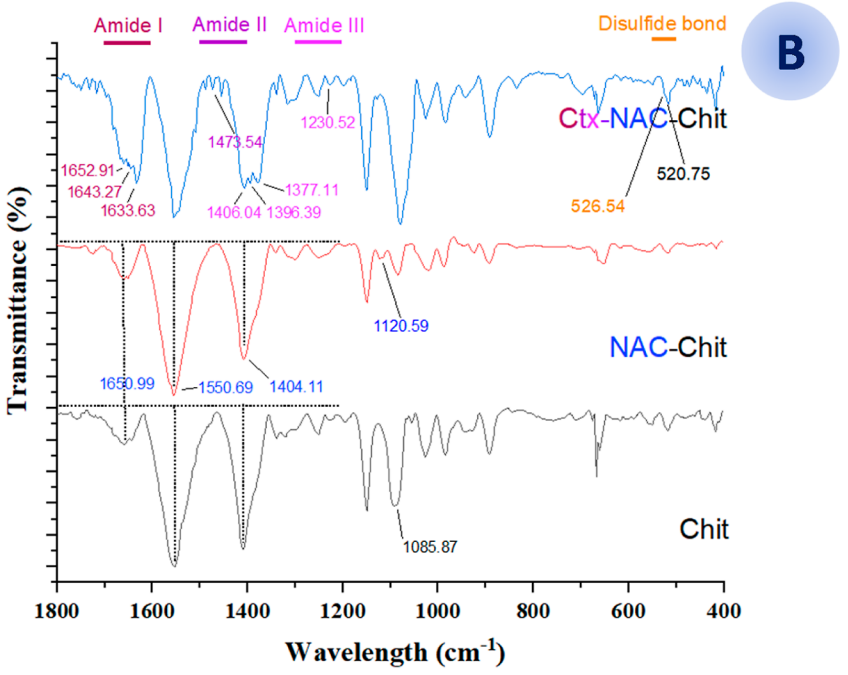


C

| Sample | Peak height ratio |
|---|---|
| Chit | 0.41 |
| NAC-Chit | 1.35 |
| Ctx-NAC-Chit | 0.63 |

**Figure 2.** (A) FT-IR spectroscopy applied to the conjugation stages. A view from the transmission region between 4000 and 400 $cm^{-1}$ on the microscope was chosen. Chitosan (Chit, blue), *N*-acetylcysteine-chitosan (NAC-Chit, green), and the peptide Ctx($Ile^{21}$)-Ha-Ahx-Cys conjugated with *N*-acetylcysteine (Ctx-NAC-Chit, orange). (B) FT-IR spectroscopy applied to the conjugation stages from 1800 to 400 $cm^{-1}$. Chitosan (Chit, black), *N*-acetylcysteine-chitosan (NAC-Chit, red), and the peptide Ctx($Ile^{21}$)-Ha-Ahx-Cys conjugated with *N*-acetylcysteine (Ctx-NAC-Chit, blue). In this study, the functional groups confirm the presence of a disulfide bond (S−S) that represents the link between the AMP and the NAC. Likewise, the difference in intensity between NAC-Chit (stronger) and Chit reflects stable binding on these two molecules, in addition to presenting the characteristic NAC between 2500 and 2600 $cm^{-1}$. (B) Peak height ratio from the amide I peak (1654 $cm^{-1}$)/C−O−C peak (1083 $cm^{-1}$) of conjugated chitosan films.



https://doi.org/10.1021/acsomega.2c02570
*ACS Omega* 2022, 7, 28238−28247

**Table 1. Percentage of Solubility in Water of Conjugated Chitosan Films**[a]

| ultrathin film | ultrathin film solubility in water (%)* |
|---|---|
| Chit | 11.2[a] |
| NAC-Chit | 15.8[b] |
| Ctx-NAC-Chit | 16.3[b] |

[a]Tukey's test (significant difference between mean values). *Equal letters mean that there is no significant difference.

the thermal and oxidative decomposition of chitosan, as well as the elimination of solvents.[29,30] Previous studies revealed that chitosan has weight losses of up to 44% when it reaches 300 °C, and this indicates that its modification with both NAC and Ctx(Ile$^{21}$)-Ha peptide increases the chitosan heat resistance.[29] In addition, unlike Ctx-NAC-Chit, which presented three additional critical events, six other critical mass loss events were recorded in NAC-Chit. This loss was related to carbon removal consequently generated in the second event.[31]

According to Rusu et al.[30] the DSC thermal scan showed a slight exothermic event during the first 100 °C, which could be related to the complete elimination of water from chitosan films. As hydrogels of chitosan (non-conjugated) films are amorphous materials, no relevant thermal events were recorded. However, the results show that the NAC-Chit peak shown at 269.09 °C can be associated with the chemical decomposition of chitosan conjugated both with NAC and the peptide, in agreement with He et al.[31] Other similar exothermic behaviors recorded would be associated with the relaxation of chitosan and endothermic events resulting from the decomposition of other organic components that were added to the chitosan structure.[32]

**4.5. X-ray Diffraction Analysis.** The diffraction patterns of the semi-crystalline chitosan phase show characteristic peaks in the crystal form I (CrI) region at 12.96° (2$\theta$) and crystal form II (CrII) at 17.54° (2$\theta$), whichrepresent (020) and (110) reflection planes of the crystal lattice of hydrates, respectively, and corroborate previously published results.[33,34] According to Breda et al.,[33] the decrease of 12.96° (2$\theta$) (Figure 4) may be due to a reduction in the crystalline structure, which indicates that Ctx-NAC-Chit and NAC-Chit increased in crystallinity. It

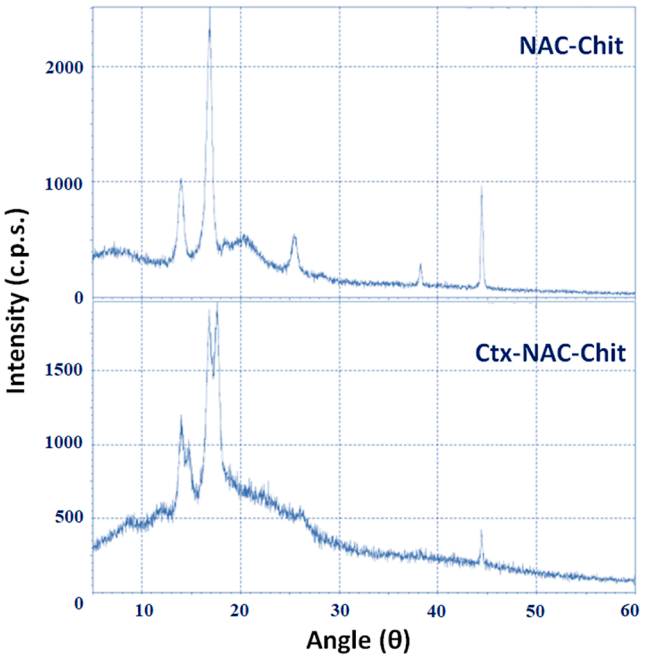


**Figure 4.** X-ray diffraction patterns of the samples conjugated with chitosan, NAC, and the Ctx(Ile$^{21}$)-Ha-Ahx-Cys peptide.

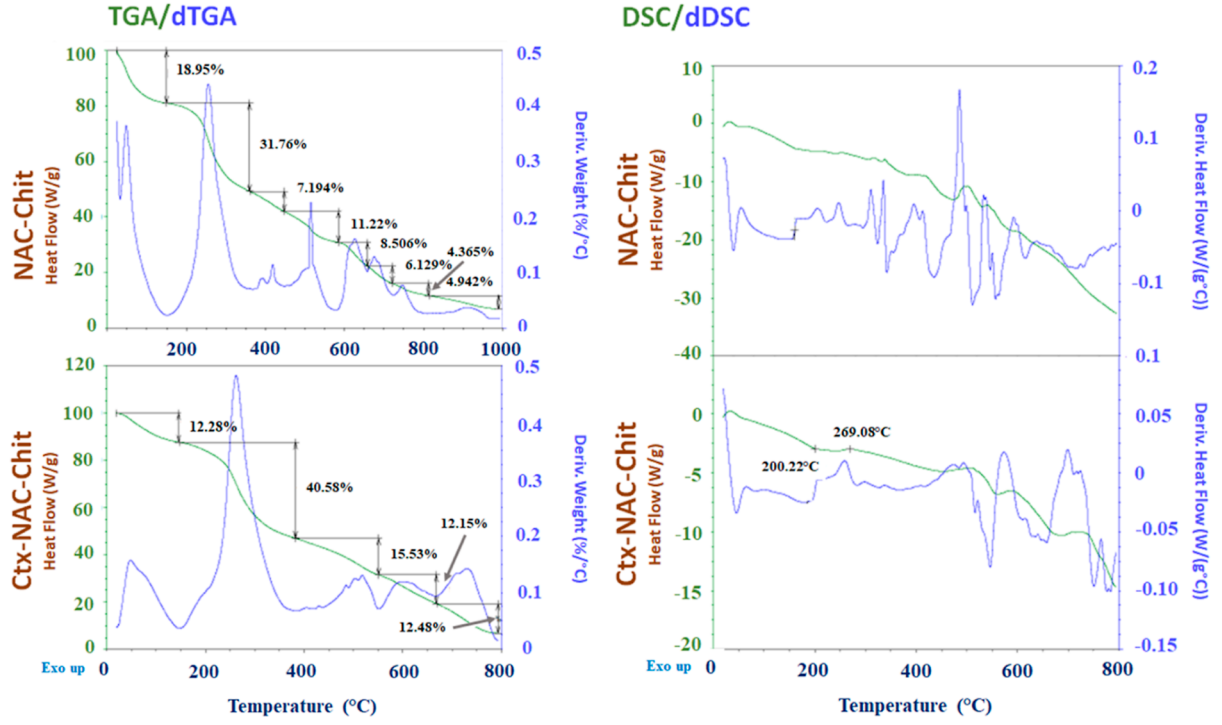


**Figure 3.** Thermograms of DSC and thermogravimetry studies, with their respective derivatives, showing the critical and important events of the conjugated chitosan samples, along with their behavior/relationship to increasing temperature.



https://doi.org/10.1021/acsomega.2c02570
ACS Omega 2022, 7, 28238−28247

was previously reported that chitin (acetylated chitosan) showed a higher peak intensity at 13.25° ($2\theta$), and this value decreased when chitosan was obtained after deacetylation.[35] The results of the Ctx-NAC-Chit conjugate were corroborated by an increase in intensity in the same region caused by the insertion of NAC. Likewise, the CrI of NAC-Chit (88.19%) was greater than that of Ctx-NAC-Chit (74.25%). In agreement with Facchinatto et al.,[36] as the acetylation increased, the CrI decreased, showing that both NAC and Ctx(Ile$^{21}$)-Ha peptide play an important role in the crystallization process.

**4.6. Morphological Analysis.** The conjugated films were morphologically characterized by SEM (Figure 5), and a

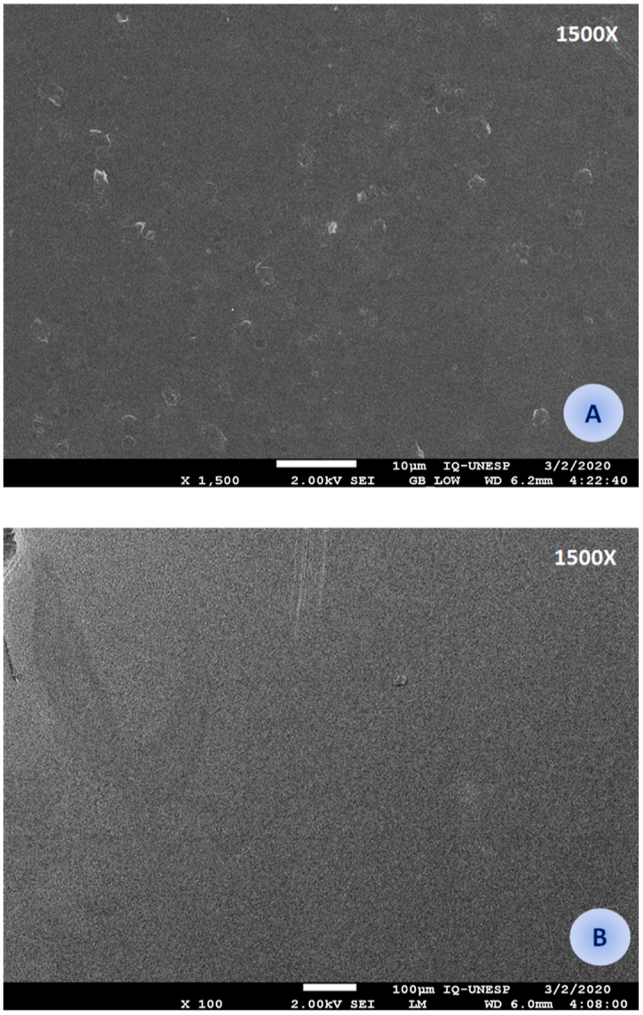


**Figure 5.** Microstructure of the thin films conjugated with NAC (A) and with the modified Ctx(Ile$^{21}$)-Ha-Ahx-Cys AMP (B).

homogeneous structure was obtained for both materials. Unlike Ctx-NAC-Chit, NAC-Chit had some crystals that could exhibit some residual sodium from chitosan precipitation using NaOH before lyophilization. Some studies on films propose the use of mild voltaic energy with electric fields of 100 V cm$^{-1}$ or temperature to avoid the presence of crystals and, thus, obtain uniform dispersion.[34,37] Another study also affirmed that the morphology of the film surface would be directly related to the preparation method/technique since an increase in energy can improve or worsen its production.[16] The micrographs shown resemble those previously reported by other researchers.[38,39]

**4.7. Mechanical Properties.** Mechanical studies, such as Ps and Eb (Table 2), were carried out using conjugated films,

**Table 2. Mechanical Properties of Conjugated Chitosan Films**

| film | Ps (MPa)[a] | Eb (%) | film thickness (mm) |
|---|---|---|---|
| Chit | 7.7 ± 0.4$^{a}$ | 14.9 ± 1.1$^{a}$ | 0.04 ± 0.02$^{a}$ |
| NAC-Chit | 1.6 ± 0.2$^{b}$ | 3.3 ± 0.2$^{b}$ | 0.03 ± 0.002$^{b}$ |
| Ctx-NAC-Chit | 2.0 ± 0.1$^{c}$ | 2.1 ± 0.04$^{b}$ | 0.03 ± 0.002$^{b}$ |

[a]Tukey's test significant difference between mean values. Different letters within the same column indicate significant differences among formulations ($p < 0.05$).

and the chitosan film was used as a control. Significant differences were found between all the conjugated films, mainly when the conjugates were compared with the non-conjugated, purified chitosan film, showing Eb and Ps-values of 4.5 and 4.8 (conjugated to NAC) up to 7 and 3.8, respectively, (conjugated to NAC + peptide) at higher times. These results show that chitosan films are most often prepared using glycerol as an intermediate and a plasticizer material, providing greater elasticity and tensile strength, mainly when it comes to food wrapping films.[40,41] These films can be potentially improved by vacuum drying or superheated steam at low pressure during their preparation as their internal structure becomes more compact. However, an excess of plasticizer might not be beneficial for its strength.[42] In addition, if the application acts as a protective cover against antimicrobials in a surgical practice accompanied by bandages, it could be very useful since it may prevent the entry of hospital pathogens.[43] Some chitosan-based bandages demonstrated successful adherence to the intestinal submucosa without sutures and preserved its structure.[44] Finally, the results indicate that this biomaterial is an ultrathin film since the peptide conjugated film (Table 2) is significantly thinner than the original chitosan-based films.

**4.8. Antibacterial Activity.** The antibacterial activity results show the effectiveness of the analyzed compounds after being synthesized. Table 3 presents the antibacterial activity of the thin films obtained (weighed in their water-free form) and homogenized in 1% acetic acid solution. In turn, the serial dilutions could indicate that the films barely conjugated with the NAC do not exhibit relevant antibacterial activity. However, after conjugation with the Ctx(Ile$^{21}$)-Ha-Ahx-Cys peptide, the antimicrobial activity is notably improved, which corroborates previously published results.[45]

MIC values obtained for the Ctx(Ile$^{21}$)-Ha AMP remain similar to those previously published.[10,11,46] Interestingly, MIC values against *S. aureus* were remarkably higher when a spacer (Ahx) and a cysteine residue were added to the original Ctx(Ile$^{21}$)-Ha peptide primary sequence. However, when NAC was grafted onto the protonated chitosan, the antibacterial activity was recovered and improved. These events could be related to the thiol groups in the cysteine residues and their instability in biological systems post synthesis.[47] Additionally, after conjugation, Ctx-NAC-Chit in a film form showed a significant difference when compared to the other tested compounds. This effect was possibly due to the inherent activity of Ctx(Ile$^{21}$)-Ha AMP and the synergy that NAC presented with other peptides such as colistin, which mainly demonstrated anti-MDR bacteria activity.[48] Chitosan can also


https://doi.org/10.1021/acsomega.2c02570
ACS Omega 2022, 7, 28238−28247

Table 3. MICs of the Synthesized Biomolecules and Films in Their Different Phases[a]

| film form | MIC (μg/mL) | | | | %HA (250 μg/mL) |
|---|---|---|---|---|---|
| | ST | PA | EC | SA | |
| chitosan (Chit) | >250 | >500 | >500 | >500 | 41.8 |
| NAC-Chit | 250 | 250 | 250 | 250 | 6.9 |
| Ctx-NAC-Chit | 32 | 2 | 16 | 16 | 39.3 |
| **compound** | | | | | |
| Ctx(Ile$^{21}$)-Ha | 64 | 64 | 16 | 32 | 100 |
| Ctx(Ile$^{21}$)-Ha-Ahx-Cys | 16 | 16 | 64 | 125 | 100 |
| gentamicin | 2 | 4 | 8 | 4 | |

[a]ST = *Salmonella* Typhimurium, PA = *Pseudomonas aeruginosa*, EC = *Escherichia coli*, SA = *Staphylococcus aureus*and %HA = percentage of hemolytic activity.

influence the elimination of microorganisms; previous reports indicated that its modification or the insertion of molecules in the $NH_2$ radical allows a larger contact surface with charges opposite to those of chitosan, allowing them to agglomerate on negative surfaces such as bacterial lipopolysaccharides.[49,50]

These results indicate that it is possible to employ much lower AMP concentrations to obtain much higher antimicrobial activities as well as biodegradable and non-toxic compounds such as chitosan.[51] As shown in Table 3, it can be inferred that chitosan-based conjugate peptides are considerably more efficient. According to Matica et al.,[3] chitosan has several mechanisms of bactericidal action, the most important of which is bacterial envelope inhibition by binding its amine groups to the cell wall and causing bacterial lysis. Therefore, AMP binding causes more potent bacterial membrane destabilization and considerably higher MICs against pathogenic bacteria.

**4.9. Hemolytic Activity.** The hemolytic activity showed that the original peptide and the analogue with the spacer-cysteine (Ctx(Ile$^{21}$)-Ha-Ahx-Cys) are highly hemolytic in excessive concentrations of MIC since the MIC values of each molecule are approximately 15 times lower than the concentration of hemolytic activity evaluated (shown in Table 3). However, it was observed that, unlike the free molecules, there was a low hemolytic activity observed for peptide conjugation. This would indicate that a formulation using MIC values would be sufficient for dermatological application in order to avoid hemolysis and prevent the entry of pathogens into open wounds.[52] Likewise, this formulation can be a promising protective film for foods since other films previously reported in the literature presented values above those reported in this study.[53−55]

## 5. CONCLUSIONS

As the discovery of new biomaterials with potential antimicrobial activity is being prioritized, this study presents the development of a new conjugated Ctx(Ile$^{21}$)-Ha peptide based on chitosan with improved antibacterial activities. In addition, the compound showed promising results regarding the formation of an ultrathin protective structure and stable films, which were properly and physicochemically characterized. These results corroborate the hypothesis that lower peptide concentrations can be useful for avoiding the spread of bacteria that cause major public health concerns. Therefore, the findings demonstrate that the adequate structural union of *N*-acetylcysteine in chitosan does not present significant differences in its antimicrobial activity. However, after conjugation with the Ctx(Ile$^{21}$)-Ha AMP, the MIC values in bacteria of public health interests were reduced. Finally, due to these promising results, this research will be continued in order to obtain other biomaterials for the food and technology sectors and/or usable hydrogel films to prevent cross-contamination through surgical procedures conferred by the ultrathin thickness of the chitosan conjugates.

## AUTHOR INFORMATION


### Corresponding Author

**Eduardo Festozo Vicente** − *School of Sciences and Engineering, São Paulo State University (Unesp), Tupã 17602-496 São Paulo, Brazil;* orcid.org/0000-0002-9154-3574; Phone: +551434044262; Email: eduardo.vicente@unesp.br

### Authors

**Cesar Augusto Roque-Borda** − *School of Pharmaceutical Sciences, São Paulo State University (Unesp), Araraquara 14801-902 São Paulo, Brazil; Vicerrectorado de Investigación, Universidad Católica de Santa María (UCSM), Arequipa 04013, Peru;* orcid.org/0000-0002-9262-0383

**Bruna Fernandes Antunes** − *School of Biotechnology in Regenerative Medicine and Medicinal Chemistry, University of Araraquara (UNIARA), Araraquara 14801-320 São Paulo, Brazil*

**Anna Beatriz Toledo Borgues** − *School of Pharmaceutical Sciences, São Paulo State University (Unesp), Araraquara 14801-902 São Paulo, Brazil*

**Janaína Teixeira Costa de Pontes** − *School of Pharmaceutical Sciences, São Paulo State University (Unesp), Araraquara 14801-902 São Paulo, Brazil*

**Andréia Bagliotti Meneguin** − *School of Pharmaceutical Sciences, São Paulo State University (Unesp), Araraquara 14801-902 São Paulo, Brazil*

**Marlus Chorilli** − *School of Pharmaceutical Sciences, São Paulo State University (Unesp), Araraquara 14801-902 São Paulo, Brazil*

**Eliane Trovatti** − *School of Biotechnology in Regenerative Medicine and Medicinal Chemistry, University of Araraquara (UNIARA), Araraquara 14801-320 São Paulo, Brazil;* orcid.org/0000-0002-0495-8115

**Silvio Rainho Teixeira** − *School of Technology and Sciences, São Paulo State University (Unesp), Presidente Prudente 19034-589 São Paulo, Brazil*

**Fernando Rogério Pavan** − *School of Pharmaceutical Sciences, São Paulo State University (Unesp), Araraquara 14801-902 São Paulo, Brazil*

Complete contact information is available at: https://pubs.acs.org/10.1021/acsomega.2c02570




https://doi.org/10.1021/acsomega.2c02570
ACS Omega 2022, 7, 28238−28247

### Author Contributions

C.A.R.B.: writing—original draft, investigation, result analysis, and performance of all the tests and applied techniques. B.F.A. and E.T.: investigation and development of chitosan conjugates. J.T.C.d.P., A.B.T.B., and F.R.P.: antibacterial activities. A.B.M. and M.C.: mechanical properties. S.R.T.: thin-film characterization by DSC/TGA and XRD. E.F.V.: conceptualization, development, supervision, funding acquisition, article reviewing, and writing.

### Notes

The authors declare no competing financial interest.

FOOTNOTE: We cite in memory of Mrs. Anna Beatriz Toledo Borges, member of the Tuberculosis Research Laboratory and scientific initiation researcher of PIBIC-CNPq/Brazil.

## ■ ACKNOWLEDGMENTS

This work was developed with the support of São Paulo Research Foundation/FAPESP (process numbers 2016/00446-7 and 2020/13497-4) and scholarships (process numbers 2018/25707-3 and 2020/16573-3). We thank the technical assistants of the Laboratory of Chemistry and Biochemistry of São Paulo State University (UNESP), School of Sciences and Engineering, Tupã, the research group "Peptides: Synthesis, Optimization, and Applied Studies—PeSEAp", and Laura Gleriani from the Tuberculosis Lab for their continuous support.

## ■ REFERENCES

(1) Li, S.; Zhou, J.; Huang, Y. H.; Roy, J.; Zhou, N.; Yum, K.; Sun, X.; Tang, L. Injectable Click Chemistry-Based Bioadhesives for Accelerated Wound Closure. *Acta Biomater.* **2020**, *110*, 95−104.

(2) Rabea, E. I.; Badawy, M. E. T.; Stevens, C. V.; Smagghe, G.; Steurbaut, W. Chitosan as Antimicrobial Agent: Applications and Mode of Action. *Biomacromolecules* **2003**, *4*, 1457−1465.

(3) Matica, M. A.; Aachmann, F. L.; Tøndervik, A.; Sletta, H.; Ostafe, V. Chitosan as a Wound Dressing Starting Material: Antimicrobial Properties and Mode of Action. *Int. J. Mol. Sci.* **20192019**, *20*, 5889.

(4) Sahariah, P.; Másson, M. Antimicrobial Chitosan and Chitosan Derivatives: A Review of the Structure-Activity Relationship. *Biomacromolecules* **2017**, *18*, 3846−3868.

(5) Schmitz, T.; Grabovac, V.; Palmberger, T. F.; Hoffer, M. H.; Bernkop-Schnürch, A. Synthesis and Characterization of a Chitosan-N-Acetyl Cysteine Conjugate. *Int. J. Pharm.* **2008**, *347*, 79−85.

(6) Silveira, R. F.; Roque-Borda, C. A.; Vicente, E. F. Antimicrobial Peptides as a Feed Additive Alternative to Animal Production, Food Safety and Public Health Implications: An Overview. *Anim. Nutr.* **2021**, *7*, 896−904.

(7) Hancock, R. E. W.; Alford, M. A.; Haney, E. F. Antibiofilm Activity of Host Defence Peptides: Complexity Provides Opportunities. *Nat. Rev. Microbiol.* **2021**, *19*, 786−797.

(8) Haney, E. F.; Straus, S. K.; Hancock, R. E. W. Reassessing the Host Defense Peptide Landscape. *Front. Chem.* **2019**, *7*, 43.

(9) Nagarajan, D.; Nagarajan, T.; Roy, N.; Kulkarni, O.; Ravichandran, S.; Mishra, M.; Chakravortty, D.; Chandra, N. Computational Antimicrobial Peptide Design and Evaluation against Multidrug-Resistant Clinical Isolates of Bacteria. *J. Biol. Chem.* **2018**, *293*, 3492−3509.

(10) Vicente, E. F.; Basso, L. G. M.; Cespedes, G. F.; Lorenzón, E. N.; Castro, M. S.; Mendes-Giannini, M. J. S.; Costa-Filho, A. J.; Cilli, E. M. Dynamics and Conformational Studies of TOAC Spin Labeled Analogues of Ctx(Ile21)-Ha Peptide from Hypsiboas Albopunctatus. *PLoS One* **2013**, *8*, No. e60818.

(11) Roque-Borda, C. A.; Silva, H. R. L.; Crusca Junior, E.; Serafim, J. A.; Meneguin, A. B.; Chorilli, M.; Macedo, W. C.; Teixeira, S. R.; Guastalli, E. A. L.; Soares, N. M.; Blair, J. M.; Pikramenou, Z.; Vicente, E. F. Alginate-Based Microparticles Coated with HPMCP/AS Cellulose-Derivatives Enable the Ctx(Ile21)-Ha Antimicrobial Peptide Application as a Feed Additive. *Int. J. Biol. Macromol.* **2021**, *183*, 1236−1247.

(12) Roque-Borda, C. A.; Pereira, L. P.; Guastalli, E. A. L.; Soares, N. M.; Mac-Lean, P. A. B.; Salgado, D. D.; Meneguin, A. B.; Chorilli, M.; Vicente, E. F. HPMCP-Coated Microcapsules Containing the Ctx(Ile21)-Ha Antimicrobial Peptide Reduce the Mortality Rate Caused by Resistant Salmonella Enteritidis in Laying Hens. *Antibiotics* **2021**, *10*, 616.

(13) Drayton, M.; Kizhakkedathu, J. N.; Straus, S. K. Towards Robust Delivery of Antimicrobial Peptides to Combat Bacterial Resistance. *Molecules* **2020**, *25*, 3048.

(14) Li, W.; Separovic, F.; O'Brien-Simpson, N. M.; Wade, J. D. Chemically Modified and Conjugated Antimicrobial Peptides against Superbugs. *Chem. Soc. Rev.* **2021**, *50*, 4932−4973.

(15) Costa, F. M. T. A.; Maia, S. R.; Gomes, P. A. C.; Martins, M. C. L. Dhvar5 Antimicrobial Peptide (AMP) Chemoselective Covalent Immobilization Results on Higher Antiadherence Effect than Simple Physical Adsorption. *Biomaterials* **2015**, *52*, 531−538.

(16) García, M. A.; Pinotti, A.; Martino, M.; Zaritzky, N. Electrically Treated Composite FILMS Based on Chitosan and Methylcellulose Blends. *Food Hydrocolloids* **2009**, *23*, 722−728.

(17) Roque-Borda, C. A.; da Silva, P.; Rodrigues, M. C.; Azevedo, M. C.; Di Filippo, R. B.; Duarte, L.; Chorilli, J. L.; Festozo Vicente, M.; Pavan, E.; Pavan, F. R. Challenge in the Discovery of New Drugs: Antimicrobial Peptides against WHO-List of Critical and High-Priority Bacteria. *Pharmaceutics* **2021**, *13*, 773.

(18) Struszczyk, H. Microcrystalline Chitosan. I. Preparation and Properties of Microcrystalline Chitosan. *J. Appl. Polym. Sci.* **1987**, *33*, 177−189.

(19) Bagliotti Meneguin, A.; Stringhetti Ferreira Cury, B.; Evangelista, R. C. Films from Resistant Starch-Pectin Dispersions Intended for Colonic Drug Delivery. *Carbohydr. Polym.* **2014**, *99*, 140−149.

(20) Clinical and Laboratory Standards Institute. Standards for Antimicrobial Susceptibility Testing. *M100 Performance Standards for Antimicrobial Susceptibility Testing*, 28th ed., 2018; Vol. *1*.

(21) Serrano, D. R.; Hernández, L.; Fleire, L.; González-Alvarez, I.; Montoya, A.; Ballesteros, M. P.; Dea-Ayuela, M. A.; Miró, G.; Bolás-Fernández, F.; Torrado, J. J. Hemolytic and Pharmacokinetic Studies of Liposomal and Particulate Amphotericin B Formulations. *Int. J. Pharm.* **2013**, *447*, 38−46.

(22) Gonciarz, W.; Lechowicz, Ł.; Urbaniak, M.; Kaca, W.; Chmiela, M. Attenuated Total Reflectance Fourier Transform Infrared Spectroscopy (FTIR) and Artificial Neural Networks Applied to Investigate Quantitative Changes of Selected Soluble Biomarkers, Correlated with H. Pylori Infection in Children and Presumable Consequent Delayed Growth. *J. Clin. Med.* **20202020**, *9*, 3852.

(23) Lan, Q.; Di, D.; Wang, S.; Zhao, Q.; Gao, Y.; Chang, D.; Jiang, T. Chitosan-N-acetylcysteine modified HP-$\beta$-CD inclusion complex as a potential ocular delivery system for anti-cataract drug: Quercetin. *J. Drug Deliv. Sci. Technol.* **2020**, *55*, 101407.

(24) Brandt, N. N.; Chikishev, A. Y.; Mankova, A. A.; Sakodynskaya, I. K. Effect of Thermal Denaturation, Inhibition, and Cleavage of Disulfide Bonds on the Low-Frequency Raman and FTIR Spectra of Chymotrypsin and Albumin. *J. Biomed. Opt.* **2014**, *20*, 051015.

(25) Staroszczyk, H.; Sztuka, K.; Wolska, J.; Wojtasz-Pająk, A.; Kołodziejska, I. Interactions of Fish Gelatin and Chitosan in Uncrosslinked and Crosslinked with EDC Films: FT-IR Study. *Spectrochim. Acta, Part A* **2014**, *117*, 707−712.

(26) Güler, G.; Džafić, E.; Vorob'ev, M. M.; Vogel, V.; Mäntele, W. Real Time Observation of Proteolysis with Fourier Transform Infrared (FT-IR) and UV-Circular Dichroism Spectroscopy: Watching a Protease Eat a Protein. *Spectrochim. Acta, Part A* **2011**, *79*, 104−111.

(27) Ricciardi, V.; Portaccio, M.; Manti, L.; Lepore, M. An FTIR Microspectroscopy Ratiometric Approach for Monitoring X-Ray



https://doi.org/10.1021/acsomega.2c02570
*ACS Omega* 2022, 7, 28238−28247

Irradiation Effects on SH-SY5Y Human Neuroblastoma Cells. *Appl. Sci.* **2020**, *10*, 2974.
(28) Adil, M.; Amin, S.; Mohtashim, M. N-acetylcysteine in dermatology. *Indian J. Dermatol. Venereol. Leprol.* **2018**, *84*, 652.
(29) Valderruten, N. E.; Valverde, J. D.; Zuluaga, F.; Ruiz-Durántez, E. Synthesis and Characterization of Chitosan Hydrogels Cross-Linked with Dicarboxylic Acids. *React. Funct. Polym.* **2014**, *84*, 21−28.
(30) Rusu, A. G.; Popa, M. I.; Lisa, G.; Vereştiuc, L. Thermal Behavior of Hydrophobically Modified Hydrogels Using TGA/FTIR/MS Analysis Technique. *Thermochim. Acta* **2015**, *613*, 28−40.
(31) He, L.; Xue, R.; Yang, D.; Liu, Y.; Song, R. EFFECTS OF BLENDING CHITOSAN WITH PEG ON SURFACE MORPHOLOGY, CRYSTALLIZATION AND THERMAL PROPERTIES. *Chin. J. Polym. Sci.* **2009**, *27*, 501.
(32) Kaya, M.; Khadem, S.; Cakmak, Y. S.; Mujtaba, M.; Ilk, S.; Akyuz, L.; Salaberria, A. M.; Labidi, J.; Abdulqadir, A. H.; Deligöz, E. Antioxidative and Antimicrobial Edible Chitosan Films Blended with Stem, Leaf and Seed Extracts of Pistacia Terebinthus for Active Food Packaging. *RSC Adv.* **2018**, *8*, 3941−3950.
(33) Breda, C. A.; Morgado, D. L.; Assis, O. B. G.; Duarte, M. C. T. Processing and Characterization of Chitosan Films with Incorporation of Ethanolic Extract from "Pequi" Peels. *Macromol. Res.* **2017**, *25*, 1049−1056.
(34) Souza, B. W. S.; Cerqueira, M. A.; Martins, J. T.; Casariego, A.; Teixeira, J. A.; Vicente, A. A. Influence of Electric Fields on the Structure of Chitosan Edible Coatings. *Food Hydrocolloids* **2010**, *24*, 330−335.
(35) Baskar, D.; Sampath Kumar, T. S. Effect of Deacetylation Time on the Preparation, Properties and Swelling Behavior of Chitosan Films. *Carbohydr. Polym.* **2009**, *78*, 767−772.
(36) Facchinatto, W. M.; dos Santos, D. M.; Fiamingo, A.; Bernardes-Filho, R.; Campana-Filho, S. P.; de Azevedo, E. R.; Colnago, L. A. Evaluation of Chitosan Crystallinity: A High-Resolution Solid-State NMR Spectroscopy Approach. *Carbohydr. Polym.* **2020**, *250*, 116891.
(37) Casariego, A.; Souza, B. W. S.; Cerqueira, M. A.; Teixeira, J. A.; Cruz, L.; Díaz, R.; Vicente, A. A. Chitosan/clay films' properties as affected by biopolymer and clay micro/nanoparticles' concentrations. *Food Hydrocolloids* **2009**, *23*, 1895−1902.
(38) Mousavi, S. R.; Asghari, M.; Mahmoodi, N. M. Chitosan-Wrapped Multiwalled Carbon Nanotube as Filler within PEBA Thin Film Nanocomposite (TFN) Membrane to Improve Dye Removal. *Carbohydr. Polym.* **2020**, *237*, 116128.
(39) Zhang, W.; Li, X.; Jiang, W. Development of Antioxidant Chitosan Film with Banana Peels Extract and Its Application as Coating in Maintaining the Storage Quality of Apple. *Int. J. Biol. Macromol.* **2020**, *154*, 1205−1214.
(40) Rubilar, J. F.; Cruz, R. M. S.; Silva, H. D.; Vicente, A. A.; Khmelinskii, I.; Vieira, M. C. Physico-Mechanical Properties of Chitosan Films with Carvacrol and Grape Seed Extract. *J. Food Eng.* **2013**, *115*, 466−474.
(41) Thakhiew, W.; Devahastin, S.; Soponronnarit, S. Effects of Drying Methods and Plasticizer Concentration on Some Physical and Mechanical Properties of Edible Chitosan Films. *J. Food Eng.* **2010**, *99*, 216−224.
(42) Mayachiew, P.; Devahastin, S. Effects of Drying Methods and Conditions on Release Characteristics of Edible Chitosan Films Enriched with Indian Gooseberry Extract. *Food Chem.* **2010**, *118*, 594−601.
(43) Tavares, W. S.; Tavares-Júnior, A. G.; Otero-Espinar, F. J.; Martín-Pastor, M.; Sousa, F. F. O. Design of Ellagic Acid-Loaded Chitosan/Zein Films for Wound Bandaging. *J. Drug Delivery Sci. Technol.* **2020**, *59*, 101903.
(44) Lauto, A. Integration of Extracellular Matrix with Chitosan Adhesive Film for Sutureless Tissue Fixation. *Lasers Surg. Med.* **2009**, *41*, 366−371.
(45) Petrin, T. H. C.; Fadel, V.; Martins, D. B.; Dias, S. A.; Cruz, A.; Sergio, L. M.; Arcisio-Miranda, M.; Castanho, M. A. R. B.; dos Santos Cabrera, M. P. Synthesis and Characterization of Peptide-Chitosan Conjugates (PepChis) with Lipid Bilayer Affinity and Antibacterial Activity. *Biomacromolecules* **2019**, *20*, 2743−2753.
(46) Ferreira Cespedes, G.; Nicolas Lorenzon, E.; Festozo Vicente, E.; Jose Soares Mendes-Giannini, M.; Fontes, W.; de Souza Castro, M.; Maffud Cilli, E. Mechanism of Action and Relationship Between Structure and Biological Activity of Ctx-Ha: A New Ceratotoxin-like Peptide from Hypsiboas Albopunctatus. *Protein Pept. Lett.* **2012**, *19*, 596−603.
(47) Liu, D.; Li, J.; Pan, H.; He, F.; Liu, Z.; Wu, Q.; Bai, C.; Yu, S.; Yang, X. Potential Advantages of a Novel Chitosan-N-Acetylcysteine Surface Modified Nanostructured Lipid Carrier on the Performance of Ophthalmic Delivery of Curcumin. *Sci. Rep.* **2016**, *6*, 1−14.
(48) De Angelis, M.; Mascellino, M. T.; Miele, M. C.; Al Ismail, D.; Colone, M.; Stringaro, A.; Vullo, V.; Venditti, M.; Mastroianni, C. M.; Oliva, A. High Activity of N-Acetylcysteine in Combination with Beta-Lactams against Carbapenem-Resistant Klebsiella Pneumoniae and Acinetobacter Baumannii. *Antibiotics* **2022**, *11*, 225.
(49) Barbosa, M.; Costa, F.; Monteiro, C.; Duarte, F.; Martins, M. C. L.; Gomes, P. Antimicrobial Coatings Prepared from Dhvar-5-Click-Grafted Chitosan Powders. *Acta Biomater.* **2019**, *84*, 242−256.
(50) Ardean, C.; Davidescu, C. M.; Nemeş, N. S.; Negrea, A.; Ciopec, M.; Duteanu, N.; Negrea, P.; Duda-Seiman, D.; Musta, V. Factors Influencing the Antibacterial Activity of Chitosan and Chitosan Modified by Functionalization. *Int. J. Mol. Sci.* **2021**, *22*, 7449.
(51) Koc, B.; Akyuz, L.; Cakmak, Y. S.; Sargin, I.; Salaberria, A. M.; Labidi, J.; Ilk, S.; Cekic, F. O.; Akata, I.; Kaya, M. Production and Characterization of Chitosan-Fungal Extract Films. *Food Biosci.* **2020**, *35*, 100545.
(52) Thao, N. T. T.; Wijerathna, H. M. S. M.; Kumar, R. S.; Choi, D.; Dananjaya, S. H. S.; Attanayake, A. P. Preparation and Characterization of Succinyl Chitosan and Succinyl Chitosan Nanoparticle Film: In Vitro and in Vivo Evaluation of Wound Healing Activity. *Int. J. Biol. Macromol.* **2021**, *193*, 1823−1834.
(53) Naeeji, N.; Shahbazi, Y.; Shavisi, N. Vitro Antimicrobial Effect of Basil Seed Mucilage-Chitosan Films Containing Ziziphora Clinopodioides Essential Oil and MgO Nanoparticles. *Nanomed. Res. J.* **2020**, *5*, 225−233.
(54) De Souza, V. V. M. A.; Crippa, B. L.; De Almeida, J. M.; Iacuzio, R.; Setzer, W. N.; Sharifi-Rad, J.; Silva, N. C. C. Synergistic Antimicrobial Action and Effect of Active Chitosan-Gelatin Biopolymeric Films Containing Thymus Vulgaris, Ocimum Basilicum and Origanum Majorana Essential Oils against Escherichia Coli and Staphylococcus Aureus. *Cell. Mol. Biol.* **2020**, *66*, 214−223.
(55) Kim, Y. H.; Kim, G. H.; Yoon, K. S.; Shankar, S.; Rhim, J.-W. Comparative Antibacterial and Antifungal Activities of Sulfur Nanoparticles Capped with Chitosan. *Microb. Pathog.* **2020**, *144*, 104178.


https://doi.org/10.1021/acsomega.2c02570
*ACS Omega* 2022, 7, 28238−28247